Direct measurement of carbon dioxide removal due to enhanced weathering

Ella Milliken[1]*, Alex Woodley[2], Noah J. Planavsky[1,3]

1. Department of Earth & Planetary Sciences, Yale University, New Haven, CT, 06520
2. Department of Crop and Soil Sciences and NC Plant Sciences Initiative, North Carolina State University, Raleigh, NC, 27695
3. Yale Center For Natural Carbon Capture, Yale University, New Haven, CT, 06520

Corresponding Author: Ella Milliken, ella.milliken@yale.edu

Abstract

Enhanced weathering (EW) is a durable carbon removal strategy with clear pathways to produce significant global supply on a decadal scale. Despite increasing interest and investment in this process, there have been limited direct, continuous observations of instantaneous carbon removal rates from feedstock dissolution. In this study, we monitor a soybean plot amended with basalt in Southeast Virginia using continuous in-soil CO_2 monitors, a method not previously applied in agricultural EW trials. We provide clear evidence of CO_2 flux reduction within the soil profile, equivalent to 1.04 tCO_2 ha^{-1} yr^{-1}. This removal is most substantial in the growing season, following significant rain pulses. This work supports that direct, continuous gas-phase measurements could play an important role in advancing our understanding of biotic and abiotic influences on enhanced weathering rates, and demonstrating enhanced weathering to be a rigorous, scalable method of durable carbon removal.

Keywords: enhanced weathering, carbon dioxide removal, in-soil CO_2, gas-phase MRV, time-lag

Synopsis: This study provides direct evidence of gas-phase CO_2 removal in enhanced weathering through measured reductions in the soil CO_2 concentration profile.

Introduction

There is a significant gap between current global emissions and Paris Agreement goals to remain below 2°C of warming[1]. Carbon dioxide removal (CDR) has become incorporated in the projected greenhouse gas budgets of many nations for the coming century[2,3]. There has been accompanying global investment in durable CDR, with many countries supporting demonstration projects and developing related policy[2,4]. Despite notable advances in project deployment within the past decade, there is still a massive discrepancy between global estimates of durable CDR demand and supply[2,5–7].

Enhanced weathering (EW) is a geochemical CDR strategy with a pathway to hit gigaton-scale removal this century, with recent estimates projecting up to 0.5 $GtCO_2$ yr^{-1} of removal by 2070[8]. EW builds on our understanding of natural silicate weathering, a climatic feedback on geologic timescales. In EW deployments, crushed, reactive silicate rock is applied to terrestrial environments to foster rapid dissolution rates, ultimately increasing the alkalinity of the system by releasing major base cations[9]. The resulting pH and micronutrient increase from this reaction have been of particular interest for terrestrial agricultural systems, where low soil fertility is a persistent issue that will only be exacerbated by climate change[10–13].

Current best-practice EW field quantification methods rely on aqueous and solid phase cation measurements to quantify CDR rates in EW deployments[14–16]. Aqueous phase measurements, such as porewaters or stream catchment samples, can be measured directly for total alkalinity (TA)[6,9–11]. However, generating continuous, accurate data from aqueous measurements is not currently possible, and traditional methods are labor-intensive[15]. Further, watershed signals can be highly dilute in large catchments and may require geochemical tracers to provide evidence of weathering product transport[17]. Soil-based cation mass balance approaches will intrinsically give a maximum estimation of CDR within the system, and there may be significant time delays between soil signals and decreased CO_2 fluxes due to cation sorption within the soil column[18].

CO_2 gas flux measurement is an obvious complement to aqueous and solid phase methods of tracking EW rates. This method provides the most direct measure of field-scale carbon removal rates. Previously, EW gas measurements have focused on using aboveground flux chambers and eddy covariance towers to approximate dissolution. These methods have high signal-to-noise ratios due to diurnal vegetation CO_2 pulses and high surface heterogeneity, making it difficult to produce a substantial signal[19–22]. The

use of in-soil CO_2 sensors is a well-established technique for understanding changing soil carbon dynamics[23–25]. However, monitoring of in-soil CO_2 has yet to be studied in an agricultural EW system.

Here, we provide direct, gas-phase evidence of CO_2 removal within the soil profile during feedstock dissolution, using a plot-level experiment over a half-year of monitoring in Southern Virginia, USA. We use a dataset of continually logged soil CO_2 concentration ($[CO_2]$), volumetric water content (θ), temperature, and pressure to give a conservative estimate of immediate CO_2 removal due to enhanced weathering.

Materials and Methods

Site Description

The research site is located on a no-till corn-wheat-soybean agricultural farm in Clarksville, VA, in the Piedmont region of Southside Virginia. The soil across the study region is a fine, mixed, subactive, thermic, oxyaquic hapludult, with a parent material of alluvial capped felsic granite. The Ap horizon continues to 22 cm, followed by an E horizon to 40 cm, and various B horizons continuing to 130+ cm (SI Fig.1). Soils are homogenous across the study region, with 0-2% slope over the area. For the study season, winter wheat was harvested in early June and soybeans planted in late June. A Farmblox weather station providing temperature and atmospheric pressure data was installed on-site. Precipitation data for the Clarksville area was taken from the quality-controlled NOAA-NWS database, with measurements being taken every 20 minutes from a local weather station located approximately 9 miles from the research site. Regional long-term data has been logged by a local USGS weather station since 2010 (SI Fig. 2)

Following the planting of Pioneer conventional soybeans and herbicide application in June 2024, a 50 ft x 108 ft region with homogeneous soils and even prior-season growth was removed from normal practices to use for the gas monitoring array, 15 ft from a service road (SI Fig. 3). Within the plot, three 28 ft x 36 ft blocks with 6 ft alleys between them were demarcated, with each block holding sixteen 7 ft x 9 ft plots. Within each block, eight plots were randomly selected for basalt application, with a dry application rate of 44.8 t ha^{-1}. No additional fertilizer or amendments were directly applied to the field within the measurement period. There was an irrigation event and nitrogen application event on the adjoining farmland on September 6, 2024. Soybeans were harvested by hand on October 12, 2024, and rye cover crop was immediately applied.

Feedstock Analysis

Applied basalt ($Al_{0.41}Fe_{0.11}(Mg_{.16}Ca_{.14})Si_{1.17}O_2$) was sourced from Roxboro, North Carolina, with a BET SSA of 5.37 ± 1.2 $m^2\ g^{-1}$, and p80 = 89.92 μm. The BET SSA was determined via a three-point N_2 absorption analysis conducted by Particle Technology Labs, and the PSD was derived from Microtrac Sync by averaging diffraction and dynamic image analysis. The basalt has a TIC content of 0.00196 ± 0.0031 % and was analyzed using an Eltra CS-580A Analyzer. Based on XRD analysis, the basalt is comprised of 68.6% plagioclase, 14% smectite, 9.4% augite, 3.8% forsterite, 2% kaolinite, 1% chlorite, 1% talc, and 0.2% quartz. The XRD analysis was performed by ActLabs on a Bruker D8 Endeavour diffractometer equipped with Cu X-ray source and operating at the following conditions: 40 kV and 40 mA; range 4-70 deg 2θ for random specimens and 3 – 30 deg 2 θ for oriented specimens; step size 0.02 deg 2 θ; time per step 0.5 sec; fixed divergence slit, angle 0.3°; sample rotation 1 rev/sec. The PDF4/Minerals ICDD database was used for mineral identification. The quantities of the crystalline mineral phases were determined using the Rietveld method.

Soil Analysis

For each individual plot, fifteen 0-10 cm cores were collected and aggregated into one sample. Soil samples were collected in June 2024 prior to spreading, then again in October 2024 following soybean harvest. Bulk density samples were collected in December 2024 for each block, with two cores being collected for each block every 5 cm, then all values were averaged to give a 0-10 cm value for each block. The standard deviation of all bulk density samples was low ($\pm$ 0.14 g cm^{-3} for 0-10 cm, and $\pm$ 0.1 g cm^{-3} for 10-20 cm samples), reflecting high homogeneity across blocks for an agriculturally managed system. All soil samples were analyzed for organic matter (% LOI at 600°C), CEC (Mehlich-3 extraction), pH (DI water), and buffer pH (Mehlich-3 extraction).

Soil Profile Monitoring

Prior to application, 2 control and 2 basalt plots on each block, totaling 6 total control plots and 6 total basalt plots, were selected for in-soil CO_2 installation. Within these blocks, a 4-inch-diameter hole was augured to a depth of approximately 40 cm. At 10 cm, a Vaisala GMP343, fitted with a horizontal diffusion adapter, was installed pointing north within the soil profile. The probes measure up to 2% CO_2 with ± 2% measurement error. Probes were connected to Farmblox auto-loggers, which recorded raw [CO_2], filtered [CO_2], temperature, and error status every 30 seconds. This continuity in

measurement (seconds) is more conservative in frequency than other studies using comparable methods (minutes to hours)[24–27]. Auto-logging Farmblox soil moisture/temperature/electrical conductivity probes were installed at 10 cm, measuring properties every 3.5 minutes. [CO_2] at all points at 10 cm was recorded from September 2024 to February 2025.

Analysis

Soil CO_2 profiles are dynamic on a daily to weekly timescale. However, in short time intervals, the system can be assumed to behave like a steady state system. Macro-scale state shifts, such as erosion, soil production, litter production, porosity, and atmospheric CO_2, can be considered negligible changes. Micro-scale shifts, such as diurnal CO_2 production, barometric pressure, temperature, and θ, can be considered as temporal shifts that are incorporated into the flux estimation itself. Within this framework, the profile is assumed to be steady within a fixed depth and time interval. The use of the gradient method for a steady-state system has been shown to have good agreement in estimating soil CO_2 flux with continuous monitoring[24].

The CO_2 flux within the soil profile can be solved using Fick's first law:

$$F(x) = -D_s \frac{dC}{dx}$$

With D_s being given by[25,28,29]:

$$D_s = \frac{(\phi - \theta)^{2.5}}{\sqrt{\phi}} D_o$$

$$\phi = 1 - \frac{\rho_s}{\rho_r} = \epsilon + \theta$$

$$D_o = 0.00001381 \cdot \left(\frac{T}{273.15}\right)^{1.81} \cdot \left(\frac{1000}{P}\right)$$

With ϵ = air-filled porosity ($cm^3\ cm^{-3}$), ϕ = total soil porosity ($cm^3\ cm^{-3}$), ρ_s = soil bulk density ($g\ cm^{-3}$), ρ_r = particle density (2.65 $g\ cm^{-3}$), θ = measured volumetric water content (%), T = air temperature (K), and P = air pressure (Pa).

$F_{0\text{-}10}$ (μmol $CO_2\ m^{-2}\ s^{-1}$) is approximated using comparisons of atmospheric [CO_2] (421 ppm) and averaged soil [CO_2], T, and θ over 15-minute intervals. Values with [CO_2] >30000 ppm, θ > 40%, $F_{0\text{-}10}$ > 40 μmol $m^{-2}\ s^{-1}$ or a $n \leq 2$ for control and treatment were removed. Significance was determined using a Mann-Whitney test using all

replicate measurements binned in 2-hour intervals between control and treatment blocks. There was a data outage from September 26, 2024, to October 9, 2024, due to Hurricane Helene. This data was estimated by fitting an exponential curve to both control and basalt datasets, with the fit data beginning on September 15, 2024. Modeled data from these curves ($R^2_{control}$ = 0.89, R^2_{basalt}= 0.80) was then generated for the time of interest and used to calculate the cumulative flux. The remaining missing values (all with <12 hours of measurement outage) were interpolated linearly. The full dataset was then integrated to give cumulative values. Error is expressed as SEM.

Cation export efficiency

Enhanced weathering will only lead to an immediate decrease in CO_2 fluxes when the weathering products are exported below the diffusional active zone of soils. Cations moving onto sorption sites in the upper soil column temporarily reverse the weathering reaction[16]. We generate the efficiency of instantaneous (within a season) weathering product export by comparing the shift in sorbed cations relative to the CO_2 sensor-based flux estimate. Specifically, we translate the change in sorbed cation concentration between spreading (June 20, 2024) and resampling (October 20, 2024) for basalt and control treatments to a CO_2 flux estimate. For a yearly rate, this value was divided by the fraction of the year between sampling events. This does not consider cations sorbed outside of the sampled interval, making it a minimum estimate of the total cation addition into the system. Error is expressed as SEM.

Results and Discussion

Basalt dissolution is indicated in the solid phase through significant increases in pH ($p<0.0001$) and base saturation ($p=0.0007$) from June 2024 to October 2024. There was no significant change in organic matter (Fig. 1). The basalt base saturation (%) increased by 10.08 ± 5.6 %, while the control increased by 3.37 ± 7.04 %, equating to a minimum EW rate of 0.44 ± 0.04 tCO_2 ha^{-1}, or 1.34 tCO_2 $ha^{-1}yr^{-1}$ ± 0.13 tCO_2 $ha^{-1}yr^{-1}$. This base saturation estimate is conservative; it does not consider cations transported past 10 cm.

There is no significant difference in θ between treatments, but θ did vary over time, directly controlled by regional rainfall (Fig. 2a, 2b). A one-time irrigation event in early September on adjacent active farmland appeared to cause a notable rise in θ, though the volume of water applied to this experimental plot is unknown. The CO_2 flux was overall

most prominent in the growing season (August 2024 to November 2024), with rates staying relatively consistent following cover cropping (November 2024) (Fig. 2c).

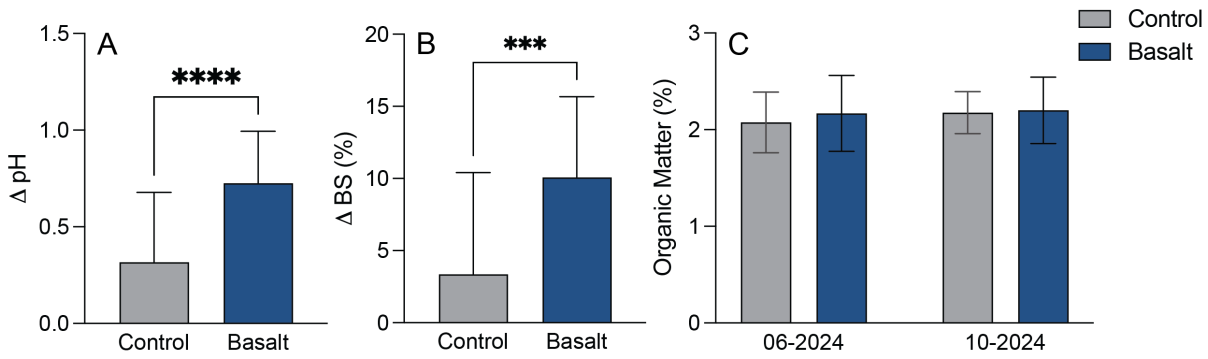

Figure 1. Agronomic soil properties prior to and following the growing season for control plots (gray) and basalt-amended plots (blue). A, B) Relative changes in soil pH and base saturation (BS %) of the post-harvest samples relative to pre-planting. C) The total organic matter (%) of the control and basalt-amended plots for each sampling month is shown. Bars represent mean ± one standard error.

The flux difference at the beginning of the year is the most prominent, with the maximal difference in flux equating to -1.23 μmol CO_2 m^{-2} s^{-1}, and an average decrease of -0.07 μmol CO_2 m^{-2} s^{-1} (Fig. 2c, 2d). This can largely be attributed to the active crop growth during this period, leading to high respiration rates from root matter, and continuous additions of organic compounds, leading to higher CO_2 production by microbes in soils[30–33]. There are also clear pulses in difference aligning with local rainfall and θ, indicating the clear relationship between weathering product transport, bicarbonate generation, and water availability within soils[34,35]. $F_{0\text{-}10}$ pulses, attributed to freeze-thaw cycling, were seen for both basalt and control within the winter months, but no differences were seen with treatment.

Periods of exceptionally high CDR demonstrate the roles that water availability, season, and crop activity play in regulating dissolution and transport rates within agricultural systems, concepts well-established in literature surrounding silicate weathering[36,37]. The empirical evidence of these connections presented here highlights the important role of land management in moderating EW rates. Specifically, a farmer's choice in planting, irrigation, and pH management, as well as inherent local climate conditions, may significantly control the dissolution rates within a deployment, as well as the retention and transport of generated bicarbonate spatially and temporally[8,34,38].

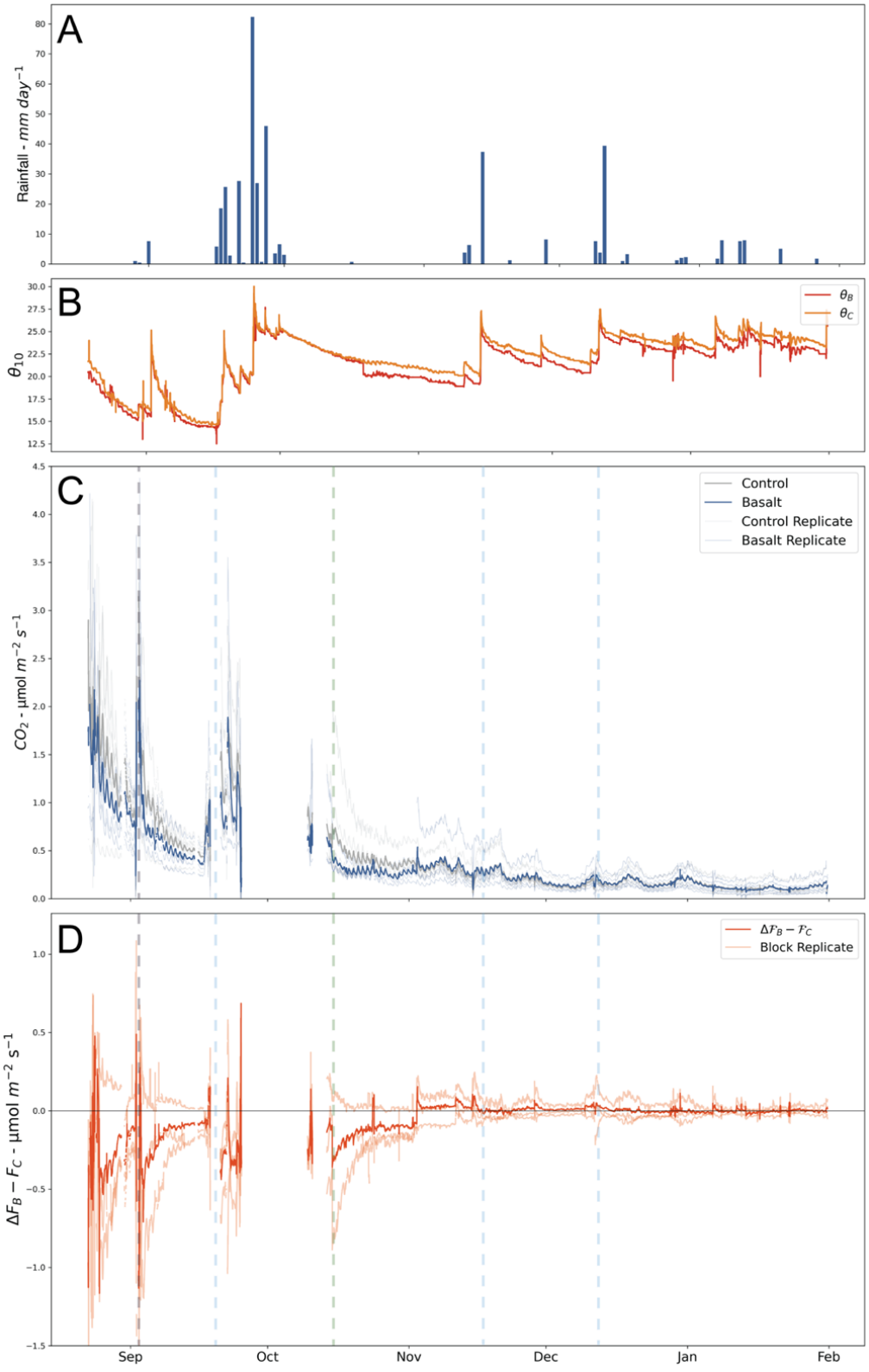

Figure 2: Comparisons of daily precipitation, volumetric water content % (θ), CO_2 flux (μmol m^{-2} s^{-1}), and difference between basalt flux (F_B) and control flux (F_C) (μmol m^{-2} s^{-1}) for control and basalt-amended

plots over the measurement period. Times marking the beginning of precipitation accumulating greater than 1 cm have been marked with blue dashed lines, and the point of harvest is marked with a green dashed line. A one-time irrigation and nitrogen application event in September on adjacent land is marked with a gray dashed line. A) Rainfall (mm day^{-1}) shows NOAA estimates for daily cumulative average rainfall from a local weather station less than 10 miles away. B) θ over time is represented as an average of monitored control (light green) and basalt (dark green) plots, respectively, with error being ≤ 1% C) The CO_2 flux (μmol m^{-2} s^{-1}) over time shows overall averages for control (gray) and basalt (blue) in bold, with individual replicate values for each plot shown. D) ΔF_B-F_C over time shows overall average subtraction in bold, with individual replicate subtractions for blocks also shown. ****$p<0.001$, ***$p<0.005$, *$p<0.05$.

At the beginning of February 2025, the cumulative control flux was 2.92 ± 0.33 tCO_2 ha^{-1}, and the cumulative basalt flux totaled 2.46 ± 0.35 tCO_2 ha^{-1} (Fig. 3a). In total, there is a cumulative decrease of 0.46 ± 0.5 tCO_2 ha^{-1}, equating to a conservative immediate EW rate of 1.04 tCO_2 ha^{-1} yr^{-1}. This estimate is lower than previous estimates of EW rates in North American field studies using basalt, but should be considered a minimum estimate, given that most cations on a short time scale are predicted to move onto sorption sites[10,20,39]. The observed shift in base saturation indicates that at least half of the cations released during EW are moved onto sorption sites in the uppermost portion of the soil column. This process releases acid into soil waters, temporarily reversing the CO_2 uptake[18,40]. Despite this reversal, the persistent decrease in $F_{0\text{-}10}$ demonstrates that there is still cation transport through these exchange sites.

This CO_2 flux-based CDR estimate highlights the dominance of CO_2 removal originating from soil respiration, as opposed to from rainwater directly. This aligns with previous studies demonstrating that mineral dissolution occurs rapidly in CO_2-rich environments as opposed to atmospheric concentrations[41]. Further, the pronounced reduction in soil CO_2 with basalt addition during the growing season highlights a clear connection between active root respiration, which elevates the pCO_2 within the soil, and decreasing CO_2 fluxes. The loss of CDR following the growing season, however, supports that reduced respiration and precipitation in cool conditions are not enough to lead to appreciable EW rates (Fig. 3b).

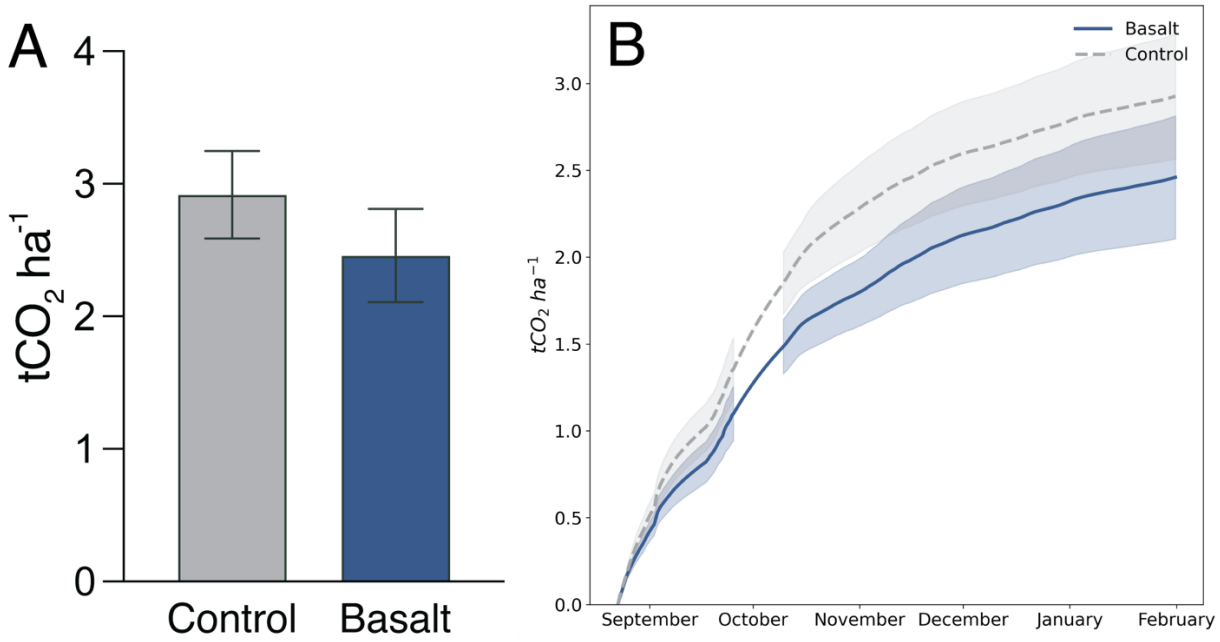

Figure 3. Cumulative emissive flux of CO_2 ($tCO_2\ ha^{-1}$) over a half-year monitoring timeframe for control (grey) and basalt (blue) amended plots. A) The total average cumulative flux at the end of January, with bars representing mean ± one standard error. B) The average cumulative change over time is shown in bold, with control and basalt SEM for the measurement period respectively shaded.

This study has a shorter analysis window than long-term EW field studies, which limits its ability to provide a robust annual CDR estimate[10,17,19,20,42]. While it is evident that the summer months make up for the most weathering over the presented monitoring period, the initial major months of weathering (June, July, August) are not included in the analysis due to a major lightning strike in July shorting several sensors, making any CDR estimates from that period unrepresentative. As such, the results of this study may not include the most reactive phase dissolution, adding to the conservative nature of the stated CDR estimate[41,42]. This estimate also assumes complete transport of bicarbonate generation through the system, with no account for potential losses downstream or re-equilibration[43,44]. Further work should include intercomparisons with data models and complementary methods to formally show relationships between dissolution rates and carbon removal estimates, both in the near-field zone and downstream.

This method is most applicable in the initial years of enhanced weathering monitoring, as there are likely to be the highest rates of dissolution, and soil organic carbon and pH fluctuations on multi-year scales may alter the comparability of respiration signals[31,45,46]. More work is necessary to understand the extent of time over which this method could be employed, the extent to which microbial respiration might change at depth with

basalt application, and the resolvability of the signal under different crop regimes[38]. Published work has shown initial evidence that respiration increases with basalt and carbonate mineral dissolution, but there have been no long-term, continuous studies focusing on respiration with silicate application[20,42]. Additionally, further work on understanding the limits of the steady-state assumption made in this initial study, particularly during periods with rapid system fluctuations caused by rapid crop growth and high precipitation, could provide further resolution in building a robust CDR estimate from this method.

The clear exponential fluctuation in EW-derived CDR, even within a month time scale, demonstrates the importance of continuous monitoring, as opposed to temporally isolated measurements, in understanding gas-phase signals. This work calls into question whether sporadic soil water or gas-phase measurements can be used to properly track carbon fluxes. This work supports that embedded soil CO_2 sensors can give robust minimum estimates of CDR rates and provides an additional line of evidence for significant rapid weathering with basalt addition to croplands. If implemented at scale, this method has the potential to provide real-time evidence of dissolution, which could increase confidence in the CDR potential for EW as it moves towards large-scale deployments.

Acknowledgements

We thank Tim Jesper Surhoff for his advice on modelling loss periods, as well as the advice of Eric Slessarev on flux analysis. We thank Varun Venkatesh for his help in soil preparation and analysis. A special thank you to Wilbourne Land and Timber for their generous and continued collaboration. We acknowledge Farmblox for their custom continuous-logging sensor design. NJP acknowledges support from Microsoft and the Yale Center for Natural Carbon Capture.

Conflict of Interest

NJP was a co-founder of the carbon dioxide removal company Lithos Carbon but has no financial ties to the company.

Supporting Information

Figure 1. Full soil profile of experimental region. Soil horizons are demarcated at each horizon boundary. Beyond 1m, the soil moved to saprolite.

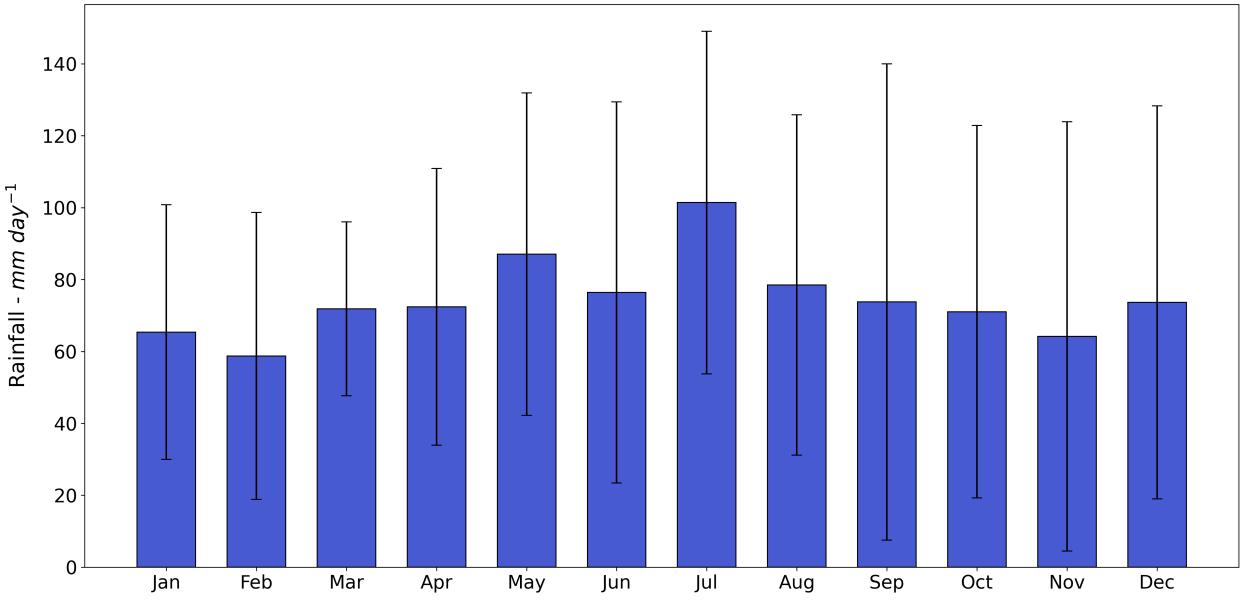

Figure 2. Local regional monthly precipitation pattern from 2011-2025. Long-term data is generated by a USGS weather station at the John H. Kerr Reservoir Dam near Boydton, VA. Average is shown by the blue bars, and standard deviation is shown by the error bars.

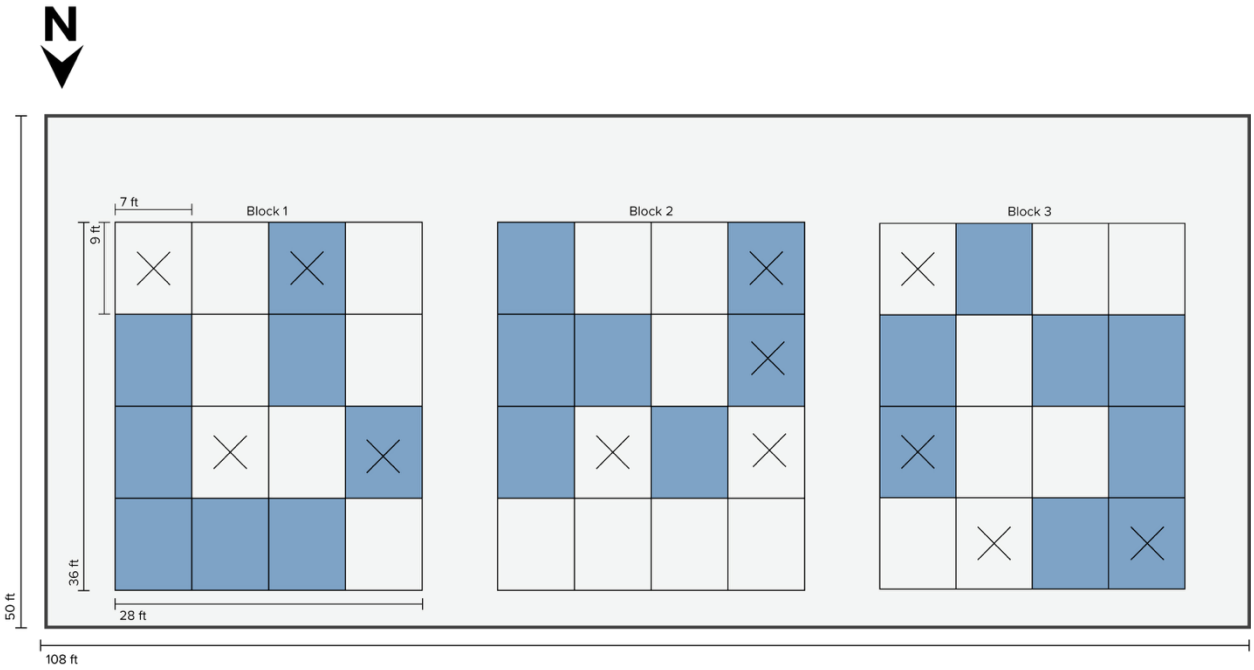

Figure 3. Experimental design of the applied region. Each application plot is an individual 7 ft by 9 ft rectangle, with sixteen plots per block in 3 total blocks, totalling 23 control plots and 25 basalt plots. In-soil CO_2 sensors, demarcated by an "X", were randomly embedded in 2 control and 2 basalt plots per block, totalling 6 basalt and 6 control replicate measurements over the area. Blocks were separated by 6 ft vertical buffers of soybeans, and a 10 ft buffer of soybeans was left between normal operations to the south. A 6 ft buffer was left to the north, with natural grasses left in the remaining 15 ft to the service road.

References

(1) *Emissions Gap Report 2024 | UNEP - UN Environment Programme.* https://www.unep.org/resources/emissions-gap-report-2024 (accessed 2025-03-10).

(2) Smith, S.; Geden, O.; Gidden, M. J.; Lamb, W. F.; Nemet, G. F.; Minx, J. C.; Buck, H.; Burke, J.; Cox, E.; Edwards, M. R.; Fuss, S.; Johnstone, I.; Müller-Hansen, F.; Pongratz, J.; Probst, B. S.; Roe, S.; Schenuit, F.; Schulte, I.; Vaughan, N. E. The State of Carbon Dioxide Removal 2024 - 2nd Edition., 2024. DOI 10.17605/OSF.IO/F85QJ.

(3) Buylova, A.; Fridahl, M.; Nasiritousi, N.; Reischl, G. Cancel (Out) Emissions? The Envisaged Role of Carbon Dioxide Removal Technologies in Long-Term National Climate Strategies. *Front. Clim.* **2021**, *3*. https://doi.org/10.3389/fclim.2021.675499.

(4) Securing Our Future: Europe's 2040 Climate Target and Path to Climate Neutrality by 2050 Building a Sustainable, Just and Prosperous Society. https://eur-lex.europa.eu/legal-content/EN/TXT/?uri=COM%3A2024%3A63%3AFIN (2024).

(5) Scott, V.; Haszeldine, R. S.; Tett, S. F. B.; Oschlies, A. Fossil Fuels in a Trillion Tonne World. *Nature Clim Change* **2015**, *5* (5), 419–423. https://doi.org/10.1038/nclimate2578.
(6) Allen, M. R.; Friedlingstein, P.; Girardin, C. A. J.; Jenkins, S.; Malhi, Y.; Mitchell-Larson, E.; Peters, G. P.; Rajamani, L. Net Zero: Science, Origins, and Implications. *Annual Review of Environment and Resources* **2022**, *47* (Volume 47, 2022), 849–887. https://doi.org/10.1146/annurev-environ-112320-105050.
(7) Dooley, K.; Keith, H.; Larson, A.; Ctacora-Vargas, G.; Carton, W.; Christinsen, K. L. The Land Gap Report 2022. https://landgap.org/2022/report (2022).
(8) Beerling, D. J.; Kantzas, E. P.; Lomas, M. R.; Taylor, L. L.; Zhang, S.; Kanzaki, Y.; Eufrasio, R. M.; Renforth, P.; Mecure, J.-F.; Pollitt, H.; Holden, P. B.; Edwards, N. R.; Koh, L.; Epihov, D. Z.; Wolf, A.; Hansen, J. E.; Banwart, S. A.; Pidgeon, N. F.; Reinhard, C. T.; Planavsky, N. J.; Val Martin, M. Transforming US Agriculture for Carbon Removal with Enhanced Weathering. *Nature* **2025**, 1–10. https://doi.org/10.1038/s41586-024-08429-2.
(9) Hartmann, J.; West, A. J.; Renforth, P.; Köhler, P.; De La Rocha, C. L.; Wolf-Gladrow, D. A.; Dürr, H. H.; Scheffran, J. Enhanced Chemical Weathering as a Geoengineering Strategy to Reduce Atmospheric Carbon Dioxide, Supply Nutrients, and Mitigate Ocean Acidification. *Reviews of Geophysics* **2013**, *51* (2), 113–149. https://doi.org/10.1002/rog.20004.
(10) Beerling, D. J.; Epihov, D. Z.; Kantola, I. B.; Masters, M. D.; Reershemius, T.; Planavsky, N. J.; Reinhard, C. T.; Jordan, J. S.; Thorne, S. J.; Weber, J.; Val Martin, M.; Freckleton, R. P.; Hartley, S. E.; James, R. H.; Pearce, C. R.; DeLucia, E. H.; Banwart, S. A. Enhanced Weathering in the US Corn Belt Delivers Carbon Removal with Agronomic Benefits. *Proc Natl Acad Sci U S A* **2024**, *121* (9), e2319436121. https://doi.org/10.1073/pnas.2319436121.
(11) Beerling, D. J.; Leake, J. R.; Long, S. P.; Scholes, J. D.; Ton, J.; Nelson, P. N.; Bird, M.; Kantzas, E.; Taylor, L. L.; Sarkar, B.; Kelland, M.; DeLucia, E.; Kantola, I.; Müller, C.; Rau, G.; Hansen, J. Farming with Crops and Rocks to Address Global Climate, Food and Soil Security. *Nature Plants* **2018**, *4* (3), 138–147. https://doi.org/10.1038/s41477-018-0108-y.
(12) Dietzen, C.; Harrison, R.; Michelsen-Correa, S. Effectiveness of Enhanced Mineral Weathering as a Carbon Sequestration Tool and Alternative to Agricultural Lime: An Incubation Experiment. *International Journal of Greenhouse Gas Control* **2018**, *74*, 251–258. https://doi.org/10.1016/j.ijggc.2018.05.007.
(13) Costa, D.; Sutter, C.; Shepherd, A.; Jarvie, H.; Wilson, H.; Elliott, J.; Liu, J.; Macrae, M. Impact of Climate Change on Catchment Nutrient Dynamics: Insights from around the World. *Environ. Rev.* **2023**, *31* (1), 4–25. https://doi.org/10.1139/er-2021-0109.
(14) Clarkson, M. O.; Larkin, C. S.; Swoboda, P.; Reershemius, T.; Suhrhoff, T. J.; Maesano, C. N.; Campbell, J. S. A Review of Measurement for Quantification of

Carbon Dioxide Removal by Enhanced Weathering in Soil. *Front. Clim.* **2024**, *6*. https://doi.org/10.3389/fclim.2024.1345224.

(15) Almaraz, M.; Bingham, N. L.; Holzer, I. O.; Geoghegan, E. K.; Goertzen, H.; Sohng, J.; Houlton, B. Z. Methods for Determining the CO2 Removal Capacity of Enhanced Weathering in Agronomic Settings. *Front. Clim.* **2022**, *4*. https://doi.org/10.3389/fclim.2022.970429.

(16) Suhrhoff, T. J.; Reershemius, T.; Wang, J.; Jordan, J. S.; Reinhard, C. T.; Planavsky, N. J. A Tool for Assessing the Sensitivity of Soil-Based Approaches for Quantifying Enhanced Weathering: A US Case Study. *Front. Clim.* **2024**, *6*. https://doi.org/10.3389/fclim.2024.1346117.

(17) Larkin, C. S.; Andrews, M. G.; Pearce, C. R.; Yeong, K. L.; Beerling, D. J.; Bellamy, J.; Benedick, S.; Freckleton, R. P.; Goring-Harford, H.; Sadekar, S.; James, R. H. Quantification of CO2 Removal in a Large-Scale Enhanced Weathering Field Trial on an Oil Palm Plantation in Sabah, Malaysia. *Front. Clim.* **2022**, *4*. https://doi.org/10.3389/fclim.2022.959229.

(18) Kanzaki, Y.; Planavsky, N. J.; Zhang, S.; Jordan, J.; Suhrhoff, T. J.; Reinhard, C. T. Soil Cation Storage Is a Key Control on the Carbon Removal Dynamics of Enhanced Weathering. *Environ. Res. Lett.* **2025**, *20* (7), 074055. https://doi.org/10.1088/1748-9326/ade0d5.

(19) Dietzen, C.; Rosing, M. T. Quantification of CO2 Uptake by Enhanced Weathering of Silicate Minerals Applied to Acidic Soils. *International Journal of Greenhouse Gas Control* **2023**, *125*, 103872. https://doi.org/10.1016/j.ijggc.2023.103872.

(20) Kantola, I. B.; Blanc-Betes, E.; Masters, M. D.; Chang, E.; Marklein, A.; Moore, C. E.; von Haden, A.; Bernacchi, C. J.; Wolf, A.; Epihov, D. Z.; Beerling, D. J.; DeLucia, E. H. Improved Net Carbon Budgets in the US Midwest through Direct Measured Impacts of Enhanced Weathering. *Global Change Biology* **2023**, *29* (24), 7012–7028. https://doi.org/10.1111/gcb.16903.

(21) Stubbs, A. R.; Paulo, C.; Power, I. M.; Wang, B.; Zeyen, N.; Wilson, S. Direct Measurement of CO2 Drawdown in Mine Wastes and Rock Powders: Implications for Enhanced Rock Weathering. *International Journal of Greenhouse Gas Control* **2022**, *113*, 103554. https://doi.org/10.1016/j.ijggc.2021.103554.

(22) Chiaravalloti, I.; Theunissen, N.; Zhang, S.; Wang, J.; Sun, F.; Ahmed, A. A.; Pihlap, E.; Reinhard, C. T.; Planavsky, N. J. Mitigation of Soil Nitrous Oxide Emissions during Maize Production with Basalt Amendments. *Front. Clim.* **2023**, *5*. https://doi.org/10.3389/fclim.2023.1203043.

(23) Vargas, R.; Detto, M.; Baldocchi, D. D.; Allen, M. F. Multiscale Analysis of Temporal Variability of Soil CO2 Production as Influenced by Weather and Vegetation. *Global Change Biology* **2010**, *16* (5), 1589–1605. https://doi.org/10.1111/j.1365-2486.2009.02111.x.

(24) Maier, M.; Schack-Kirchner, H. Using the Gradient Method to Determine Soil Gas Flux: A Review. *Agricultural and Forest Meteorology* **2014**, *192–193*, 78–95. https://doi.org/10.1016/j.agrformet.2014.03.006.
(25) Oerter, E.; Mills, J. V.; Maurer, G. E.; Lammers, L. N.; Amundson, R. Greenhouse Gas Production and Transport in Desert Soils of the Southwestern United States. *Global Biogeochemical Cycles* **2018**, *32* (11), 1703–1717. https://doi.org/10.1029/2018GB006035.
(26) Vargas, R.; Baldocchi, D. D.; Allen, M. F.; Bahn, M.; Black, T. A.; Collins, S. L.; Yuste, J. C.; Hirano, T.; Jassal, R. S.; Pumpanen, J.; Tang, J. Looking Deeper into the Soil: Biophysical Controls and Seasonal Lags of Soil CO_2 Production and Efflux. *Ecological Applications* **2010**, *20* (6), 1569–1582. https://doi.org/10.1890/09-0693.1.
(27) Hirano, T.; Kim, H.; Tanaka, Y. Long-Term Half-Hourly Measurement of Soil CO2 Concentration and Soil Respiration in a Temperate Deciduous Forest. *Journal of Geophysical Research: Atmospheres* **2003**, *108* (D20). https://doi.org/10.1029/2003JD003766.
(28) Massman, W. J. A Review of the Molecular Diffusivities of H2O, CO2, CH4, CO, O3, SO2, NH3, N2O, NO, and NO2 in Air, O2 and N2 near STP. *Atmospheric Environment* **1998**, *32* (6), 1111–1127. https://doi.org/10.1016/S1352-2310(97)00391-9.
(29) Moldrup, P.; Olesen, T.; Yamaguchi, T.; Schjønning, P.; Rolston, D. E. MODELING DIFFUSION AND REACTION IN SOILS: IX. THE BUCKINGHAM-BURDINE-CAMPBELL EQUATION FOR GAS DIFFUSIVITY IN UNDISTURBED SOIL. *Soil Science* **1999**, *164* (8), 542.
(30) Deng, H.; Sonnenthal, E.; Arora, B.; Breunig, H.; Brodie, E.; Kleber, M.; Spycher, N.; Nico, P. The Environmental Controls on Efficiency of Enhanced Rock Weathering in Soils. *Sci Rep* **2023**, *13* (1), 9765. https://doi.org/10.1038/s41598-023-36113-4.
(31) Buss, W.; Hasemer, H.; Sokol, N. W.; Rohling, E. J.; Borevitz, J. Applying Minerals to Soil to Draw down Atmospheric Carbon Dioxide through Synergistic Organic and Inorganic Pathways. *Commun Earth Environ* **2024**, *5* (1), 1–11. https://doi.org/10.1038/s43247-024-01771-3.
(32) Balland-Bolou-Bi, C.; Poszwa, A. Effect of Calco-Magnesian Amendment on the Mineral Weathering Abilities of Bacterial Communities in Acidic and Silicate-Rich Soils. *Soil Biology and Biochemistry* **2012**, *50*, 108–117. https://doi.org/10.1016/j.soilbio.2012.02.034.
(33) Verbruggen, E.; Struyf, E.; Vicca, S. Can Arbuscular Mycorrhizal Fungi Speed up Carbon Sequestration by Enhanced Weathering? *PLANTS, PEOPLE, PLANET* **2021**, *3* (5), 445–453. https://doi.org/10.1002/ppp3.10179.
(34) Cipolla, G.; Calabrese, S.; Porporato, A.; Noto, L. V. Effects of Precipitation Seasonality, Irrigation, Vegetation Cycle and Soil Type on Enhanced Weathering –

Modeling of Cropland Case Studies across Four Sites. *Biogeosciences* **2022**, *19* (16), 3877–3896. https://doi.org/10.5194/bg-19-3877-2022.

(35) Calabrese, S.; Wild, B.; Bertagni, M. B.; Bourg, I. C.; White, C.; Aburto, F.; Cipolla, G.; Noto, L. V.; Porporato, A. Nano- to Global-Scale Uncertainties in Terrestrial Enhanced Weathering. *Environ. Sci. Technol.* **2022**, *56* (22), 15261–15272. https://doi.org/10.1021/acs.est.2c03163.

(36) Berner, R. A.; Berner, E. K. Silicate Weathering and Climate. In *Tectonic Uplift and Climate Change*; Ruddiman, W. F., Ed.; Springer US: Boston, MA, 1997; pp 353–365. https://doi.org/10.1007/978-1-4615-5935-1_15.

(37) White, A. F.; Brantley, S. L. The Effect of Time on the Weathering of Silicate Minerals: Why Do Weathering Rates Differ in the Laboratory and Field? *Chemical Geology* **2003**, *202* (3), 479–506. https://doi.org/10.1016/j.chemgeo.2003.03.001.

(38) Skov, K.; Wardman, J.; Healey, M.; McBride, A.; Bierowiec, T.; Cooper, J.; Edeh, I.; George, D.; Kelland, M. E.; Mann, J.; Manning, D.; Murphy, M. J.; Pape, R.; Teh, Y. A.; Turner, W.; Wade, P.; Liu, X. Initial Agronomic Benefits of Enhanced Weathering Using Basalt: A Study of Spring Oat in a Temperate Climate. *PLOS ONE* **2024**, *19* (3), e0295031. https://doi.org/10.1371/journal.pone.0295031.

(39) Lewis, A. L.; Sarkar, B.; Wade, P.; Kemp, S. J.; Hodson, M. E.; Taylor, L. L.; Yeong, K. L.; Davies, K.; Nelson, P. N.; Bird, M. I.; Kantola, I. B.; Masters, M. D.; DeLucia, E.; Leake, J. R.; Banwart, S. A.; Beerling, D. J. Effects of Mineralogy, Chemistry and Physical Properties of Basalts on Carbon Capture Potential and Plant-Nutrient Element Release via Enhanced Weathering. *Applied Geochemistry* **2021**, *132*, 105023. https://doi.org/10.1016/j.apgeochem.2021.105023.

(40) te Pas, E. E. E. M.; Chang, E.; Marklein, A. R.; Comans, R. N. J.; Hagens, M. Accounting for Retarded Weathering Products in Comparing Methods for Quantifying Carbon Dioxide Removal in a Short-Term Enhanced Weathering Study. *Front. Clim.* **2025**, *6*. https://doi.org/10.3389/fclim.2024.1524998.

(41) Amann, T.; Hartmann, J.; Hellmann, R.; Pedrosa, E. T.; Malik, A. Enhanced Weathering Potentials—the Role of in Situ CO2 and Grain Size Distribution. *Front. Clim.* **2022**, *4*. https://doi.org/10.3389/fclim.2022.929268.

(42) Dupla, X.; Claustre, R.; Bonvin, E.; Graf, I.; Le Bayon, R.-C.; Grand, S. Let the Dust Settle: Impact of Enhanced Rock Weathering on Soil Biological, Physical, and Geochemical Fertility. *Science of The Total Environment* **2024**, *954*, 176297. https://doi.org/10.1016/j.scitotenv.2024.176297.

(43) Zhang, S.; Planavsky, N. J.; Katchinoff, J.; Raymond, P. A.; Kanzaki, Y.; Reershemius, T.; Reinhard, C. T. River Chemistry Constraints on the Carbon Capture Potential of Surficial Enhanced Rock Weathering. *Limnology and Oceanography* **2022**, *67* (S2), S148–S157. https://doi.org/10.1002/lno.12244.

(44) Kanzaki, Y.; Planavsky, N. J.; Reinhard, C. T. New Estimates of the Storage Permanence and Ocean Co-Benefits of Enhanced Rock Weathering. *PNAS Nexus* **2023**, *2* (4), pgad059. https://doi.org/10.1093/pnasnexus/pgad059.

(45) Anthony, T. L.; Jones, A. R.; Silver, W. L. Supplementing Enhanced Weathering With Organic Amendments Accelerates the Net Climate Benefit of Soil Amendments in Rangeland Soils. *AGU Advances* **2025**, *6* (2), e2024AV001480. https://doi.org/10.1029/2024AV001480.
(46) Sokol, N. W.; Sohng, J.; Moreland, K.; Slessarev, E.; Goertzen, H.; Schmidt, R.; Samaddar, S.; Holzer, I.; Almaraz, M.; Geoghegan, E.; Houlton, B.; Montañez, I.; Pett-Ridge, J.; Scow, K. Reduced Accrual of Mineral-Associated Organic Matter after Two Years of Enhanced Rock Weathering in Cropland Soils, Though No Net Losses of Soil Organic Carbon. *Biogeochemistry* **2024**, *167* (8), 989–1005. https://doi.org/10.1007/s10533-024-01160-0.